Desalination and Water Treatment
www.deswater.com
doi: 10.5004/dwt.2019.24271

158 (2019) 199–206
August

Synthesis of sodium alginate composites and their removal performances toward Pb^{2+} and Cd^{2+}

Yan Zhang[a,b,*], Feng Liang[a,b], Wenwen Qiao[b], Zhan Chen[b], Meng Li[b], Pingge Dian[b]

[a]*Henan University of Urban Construction, Henan Province Key Laboratory of Water Pollution Control and Rehabilitation Technology, Pingdingshan, Henan 467036, China, emails: zhangyan696@163.com (Y. Zhan), liangfeng@hncj.edu.cn (F. Liang)*
[b]*Department of Environmental and Municipal Engineering, Henan University of Urban Construction, Pingdingshan 467000, China, emails: 2181507@mail.dhu.edu.cn (W. Qiao), cz1343028511@163.com (Z. Chen), LM13271400605@163.com (M. Li), louis0375@163.com (P. Dian)*

Received 4 September 2018; Accepted 12 April 2019

ABSTRACT

Four adsorbents for Pb^{2+} and Cd^{2+} ions in aqueous solutions are prepared by modifying graphene oxide/sodium alginate with disodium ethylenediaminetetraacetate using different methods. Specific relative surface area, pore size analysis and the scanning electron microscopy pictures show the three-dimensional structures of these adsorbents, which possess pores of different sizes and distributions. Static adsorption experiments for Pb^{2+} and Cd^{2+} ions are carried out with the four newly synthesized adsorbents. Among them the composite of graphene oxide, sodium alginate and disodium ethylenediaminetetraacetate (SEG2), which is prepared by blending and vacuum freeze drying, has outstanding adsorption performance in removing heavy metal ions. The maximum removing rates of SEG2 toward Pb^{2+} and Cd^{2+} ions are 97.44% and 97.16%, respectively, at 298 K. This effect demonstrates that SEG2 is highly promising in the practical applications such as removing heavy metal pollutants from the water.

Keywords: Sodium alginate; Disodium ethylenediaminetetraacetate; Graphene oxide; Adsorption; Pb^{2+}; Cd^{2+}

1. Introduction

Environmental heavy metals can accumulate within the human body through the food chain. Once the quantity is over the highest allowed value, they will induce a serious of poisonous syndromes, such as headache, dizziness, sleeplessness, and joints pain. The long-term over-dose accumulation of heavy metals could even induce damages of the human neural system, digestion system, and excretory systems [1–3]. Lead and chromium are two of the most common heavy metals which are easy to accumulate and difficult to be de-composited biologically. Therefore they are listed as the top environmental pollutions that urgently require effective treatment, especially in the contaminated water.

Nowadays there are different methods to treat heavy metal pollutions, such as through chemical precipitation, ion exchange, membrane separation, electrolysis, reduction, and adsorption [4–7]. Among these methods, techniques based on adsorption have been proven to be very effective and promising [8]. To further improve the treatment efficiency and to decrease the running cost by developing novel adsorbents is therefore a very hot topic in the field of environmental protection.

Recently two-dimensional materials, such as graphene oxide (GO), have attracted tremendous attention in the field of water pollution treatment [9,10]. These kinds of materials typically refer to flat or slightly corrugated sheets with nanometer thicknesses and extended lateral dimensions,

* Corresponding author.

which can, therefore, provide extremely large specific surface areas. Furthermore, GO has corrugated carbon sheet with over half of the carbon atoms functionalized with hydroxyl and epoxy groups, and edges partially occupied by hydroxyl, carboxyl, ketone, ester and even lactol structures [11,12]. These large amounts of functional groups can serve as natural active sites for the adsorption of pollutants. Despite these advantages, the application of GO into the treatment of polluted water is limited due to its high hydrophilicity. Even the pollutants can effectively adsorb onto the GO, it is very difficult to separate them from the water body. Therefore new strategies to overcome this issue need to be developed.

In this paper, we report a new method for the treatment of heavy metal ions in polluted water using sodium alginate and GO composites. Four adsorbents for Pb^{2+} and Cd^{2+} in aqueous solutions are prepared by modifying graphene oxide/sodium alginate with disodium ethylenediaminetetraacetate. Specific surface area, pore size analysis and the scanning electron microscopy are used to characterize the morphologies and the structural properties of the novel composites. Static adsorption experiments and the removing performance toward Pb^{2+} and Cd^{2+} are compared for the composites prepared by different synthesis methods.

2. Materials and methods

2.1. Materials

Sodium alginate, calcium chloride, EDTA-2Na, lead nitrate, cadmium chloride are of analytical grade. Graphene oxide solution is purchased from Carmery Materials Technology Co. Ltd., (Taiyuan Shanxi). Twice-distilled water is used throughout the experiments. All experiments are performed at 298 K.

Inductively coupled plasma optical emission spectrometer (Optima 7000, PE company, USA) is used for determination of the concentrations of heavy metal ions. Scanning electron microscopy (Quanta450, FEI company, Netherlands) is used to characterize the material structures. Full automatic analyzer for relative surface area and porosity (ASAP2020, Micromeritics company, USA) is employed to obtain the size information of the porous structures.

2.2. Adsorbents synthesis

Four adsorbents are synthesized with the following methods:

SE: 0.4 g sodium alginate, 0.1 g EDTA and 10 mL twice-distilled water are mixed and stirred in a magnetic stirring apparatus for 4 h. Afterwards the mixture is kept in a –80°C refrigerator for 1 h and freeze-dried subsequently. Twenty-four hours later the mixture is cross-linked with 1% $CaCl_2$ solution for 30 min. The product is washed with twice-distilled water to get rid of the excess $CaCl_2$ solution, and then dried at 40°C in a vacuum oven for 2 h.

SEG1: A GO dispersion is prepared by sonicating 10 mL GO solution of 3 g L^{-1} for 2 h. Afterwards 0.4 g sodium alginate and 0.1 g EDTA are added to the GO dispersion and stirred for 4 h. Afterwards the mixture is cross-linked with 1% $CaCl_2$ solution for 30 min. The product is washed with twice-distilled water to get rid of the excess $CaCl_2$ solution, and then dried at 40°C in vacuum oven for 2 h.

SEG2: A GO dispersion is prepared by sonicating 10 mL GO solution of 3 g L^{-1} for 2 h. Afterwards 0.4 g sodium alginate and 0.1 g EDTA are added to the GO dispersion and stirred for 4 h. The mixture is kept in a –80°C refrigerator for 1 h. Subsequently, the sample is dried in a vacuum freeze drying machine. Twenty-four hours later, the mixture is cross-linked with 1% $CaCl_2$ solution for 30 min. The product is washed with twice-distilled water to get rid of the excess $CaCl_2$ solution, and then dried at 40°C in vacuum oven for 2 h.

SEG3: A GO dispersion is prepared by sonicating 10 mL GO solution of 3 g L^{-1} for 2 h. Afterwards 0.4 g sodium alginate and 0.1 g EDTA are added to the GO dispersion and stirred for 4 h. The product is filtered using vacuum filter equipped with a 0.22 μm porous membrane. The resulted composite membrane is further cross-linked with 1% $CaCl_2$ solution for 30 min. The product is washed with twice-distilled water to get rid of the excess $CaCl_2$ solution, and then dried at 40°C in vacuum oven for 2 h.

2.3. Material characterizations

The morphologies of the synthesized materials are obtained by scanning electron microscopy (FEI company, Quanta450). The relative surface areas and the porosities are characterized using a full-automatic instrument (Micromeritics, ASAP2020).

2.4. Experimental methods

The synthesized SE and SEG2 materials are cut into thin strips. The materials are then, respectively, put into the Pb^{2+} and Cd^{2+} aqueous solutions, at a concentration of 0.5 g L^{-1}. To facilitate the adsorption of the heavy metal ions, the solution mixture was shaken for 3 h in a temperature-controlled water bath shaker. Afterwards the concentrations of the Pb^{2+} and Cd^{2+} ions in the liquid phase of the solution are analyzed using inductively coupled plasma optical emission spectrometer. The amount of adsorption and the removal rate are also calculated.

For sample SEG1, the dry gel-spheres are put to the Pb^{2+} and Cd^{2+} aqueous solutions at a concentration of 0.5 g L^{-1}. Afterwards the concentrations of the Pb^{2+} and Cd^{2+} ions in the liquid phase of the solution are analyzed using inductively coupled plasma atomic emission spectroscopy. The amount of adsorption and the removal rate are also calculated.

For sample SEG3, the membranes are used as filter in vacuum filter equipped. The Pb^{2+} and Cd^{2+} aqueous solutions are filtered through the membrane. Afterwards the concentrations of the Pb^{2+} and Cd^{2+} ions in the liquid phase of the solution are analyzed using inductively coupled plasma atomic emission spectroscopy. The amount of adsorption and the removal rate are also calculated.

To calculate the amount of adsorption at the equilibrium, Eq. (1) is used.

$$q_e = \frac{\left(c_0 - c_e\right)}{m} \times V \tag{1}$$

To calculate the removal rate, Eq. (2) is used:

$$R\% = \frac{\left(c_0 - c_e\right)}{c_0} \times 100\% \tag{2}$$

where q_e is the equilibrium adsorption (mg g^{-1}), V is the solution volume (L), m is the mass of the adsorbent (g), c_0 is the initial concentration of the Pb^{2+} or Cd^{2+} ions (mg L^{-1}), c_e is the concentration of Pb^{2+} or Cd^{2+} ions at the adsorption equilibrium (mg L^{-1}), and R is the removal rate (%).

3. Results and discussions

3.1. Characterization of material morphology and porosity

To characterize the morphologies of the four synthesized materials, scanning electron microscopy (SEM) images are collected from the surface and the cross-section of the material.

As shown in Fig. 1a, the surface of SE possesses a sponge-like structure showing an inhomogeneous distribution of pores with different sizes. The SEM image (Fig. 1b) from its cross-section confirms the presence of three-dimensional porosity. The porous structure is likely resulted from the cross-link between the SA and Ca^{2+} ions. Furthermore the chemical reaction between the amino group in EDTA and the oxygen-containing group in SA could occur through the dehydration reaction.

As compared with Fig. 1a, the surface of SEG1 gel-sphere shown in Fig. 1c seems to be smoother. The SEM image taken from inside of the sphere (Fig. 1d) confirms the presence of loosely folded layer structures that are separated with irregularly shaped empty spaces. Such kind of morphology could be due to the random connections among the GO nanoparticles in the GO gel sphere through the cross-link with EDTA.

In Fig. 1e, the SEM image taken from the SEG2 surface is shown, where well-shaped porous structure can be seen. The SEM image (Fig. 1f) from the cross-section of the sample reveals vertically-arranged channel-like morphology, which are formed by well-defined folded layers. This could be due to that GO layer, wrapped with SA, forms interconnected network with Ca^{2+} ions through interactions such as the hydrogen bonds, and van der Waals forces [13]. Such kind of interactions could lead to improved mechanical strength and resilience of the material. During the drying process at the low temperature (–80°C), water is frozen and rod-like ice crystals grows from the bottom to the top surface of the membrane, inducing a relatively ordered alignment of the GO layer along the growth direction of the ice crystals. During the drying process, only the ice crystal in the membrane is sublimated leaving the channel-like morphology behind.

The surface of SEG3 (Fig. 1g) is shown to be smooth, with some nanometer-sized roughness. The inside of the sample possesses three-dimensionally connected foam-like structure, as shown in Fig. 1h. The separations among the pores are significantly smaller than the SE, SEG1, and SEG2 samples. The forming of surface roughness could be due to the highly-distorted GO layer through the cross-link with the amino-group of the EDTA molecules. Those amino groups can interact with the epoxide groups that present at random positions of the GO, inducing the distortion and folding of the GO layers [14].

The relative surface area and the porosity of the above samples are subsequently analyzed and the results are shown in Table 1. The SE shows to possess the largest surface area; whilst the SEG1 gel sphere is the smallest. Among the three samples, the SEG2 has the largest pore size, which is in good agreement with the SEM characterization.

3.2. Adsorption performances toward Pb^{2+} or Cd^{2+} ions on SE, SEG1, SEG2, and SEG3

3.2.1. SE, SEG1, SEG2

Respectively, an amount of 0.08 g SE, SEG1, SEG2 is added to 160 mL mixture solution containing Pb^{2+} and Cd^{2+} ions. The concentrations of the heavy metal ions are both 10 mg L^{-1}, and the pH value of the solution is 7. The solution mixture was shaken at room temperature for 3 h. At a different time interval, 4 mL solution is taken and the concentrations of the Pb^{2+} and Cd^{2+} ions are analyzed. The amount of adsorption at the equilibrium and the removal rates are then calculated according to Eqs. (1) and (2), respectively.

As shown in Fig. 2, with the increase of the adsorption time the removal rates SE toward Pb^{2+} (black squares) and Cd^{2+} (red points) ions are increasing gradually. In the first 30 min, the removal rates are increasing dramatically, which are gradually slowed down. After 120 min, the removal rates are steady, indicating the status of adsorption of equilibrium. At 180 min, the removal rates for Pb^{2+} and Cd^{2+} ions are 88.4% and 84.2%, respectively. The amounts of adsorption at the equilibrium are 17.68 and 16.61 mg g^{-1} for Pb^{2+} and Cd^{2+} ions, respectively. The total amount of adsorption at the equilibrium of the adsorbent SA/EDTA is 34.29 mg g^{-1}.

Similar to the experimental procedure for studying SE, 0.08 g of SEG1 gel spheres is added to 160 mL mixture solution containing Pb^{2+} and Cd^{2+} ions. The solution mixture was shaken at the room temperature for 3.5 h. As shown in Fig. 2, the removal rates of SEG1 toward Pb^{2+} and Cd^{2+} ions are increasing with the adsorption time. However, as compared with SE, it takes longer time to reach the adsorption equilibrium. Furthermore, the highest removal rates of SEG1 toward Pb^{2+} and Cd^{2+} ions within the 210 min adsorption time are only 52.62% and 51.24%, respectively. These values are more than 30% less than those for SE. Furthermore, the amounts of adsorption at the equilibrium are 10.52 and 10.25 mg g^{-1} for Pb^{2+} and Cd^{2+} ions, respectively. Hence, the total amount of adsorption at the equilibrium of the adsorbent SEG1 is 20.77 mg g^{-1}, which is significantly lower than SE.

SEG2 is a brown foam-like material. As shown in Fig. 2, similarly to SE, the removal rates of SEG2 toward Pb^{2+} and Cd^{2+} ions increase steeply in the first 40 min. and slow down gradually. At about 60 min, the increase of the removal rate begins to be steady, indicating the adsorption equilibrium. Notably, as compared with SE, the respective removal rates of SEG2 toward Pb^{2+} and Cd^{2+} ions reached 84.68% and 79.43% already in the first 40 min, which are 120 min shorter than it requires for SE. At 180 min, the removal rates toward Pb^{2+} and Cd^{2+} ions are 97.44% and 97.16%. Furthermore, the amounts of adsorption at the equilibrium are 19.74 and 19.72 mg g^{-1} for Pb^{2+} and Cd^{2+} ions, respectively. Hence, the total amount of adsorption at the equilibrium of the adsorbent SEG2 is 39.46 mg g^{-1}. These values demonstrate that outstanding performance can be achieved from SEG2 as compared with SE and SEG1.

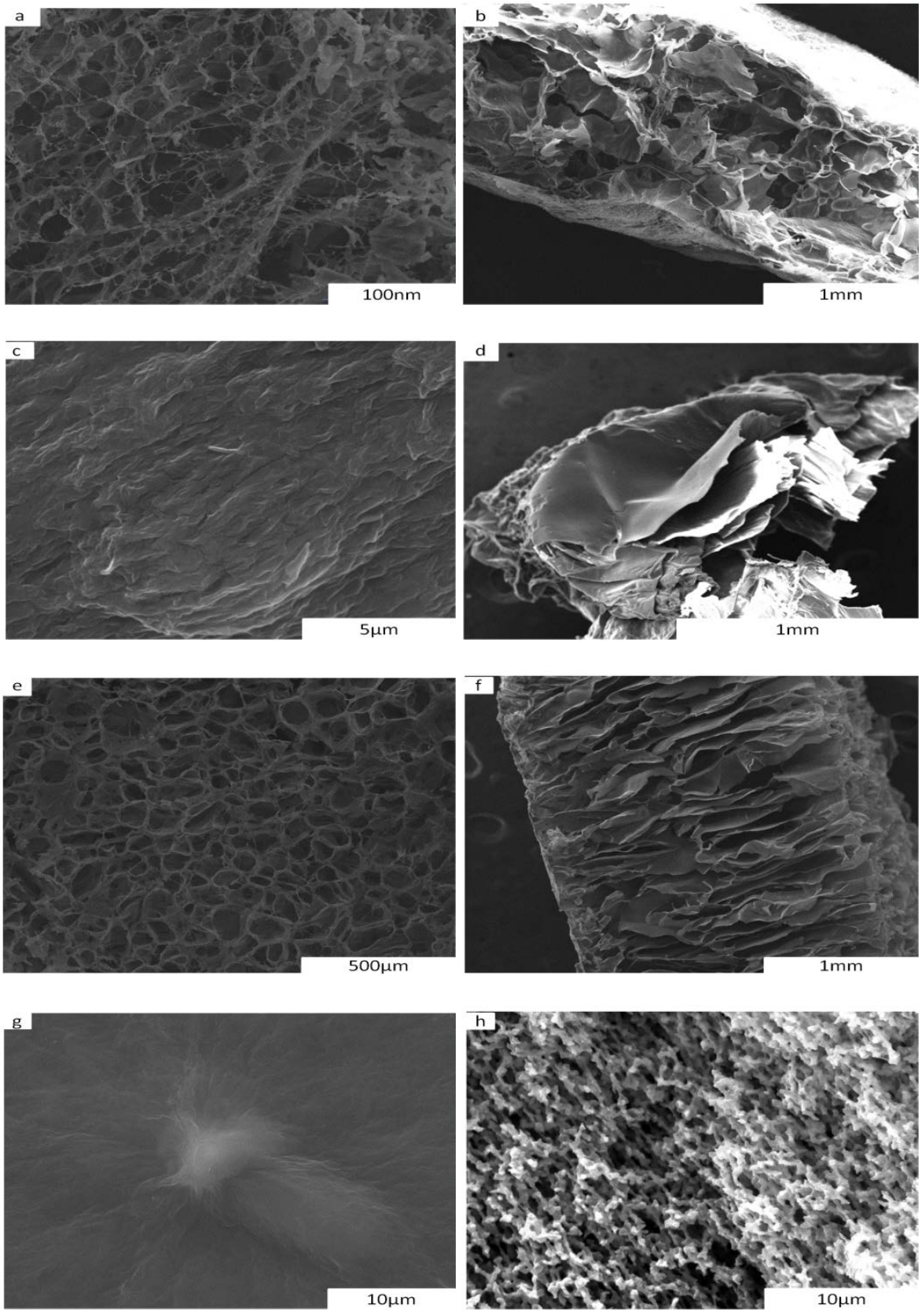

Fig. 1. SEM images taken from SE (a,b), SEG1 (c,d), SEG2 (e,f), and SEG3 (g,h). Left column: surface morphology. Right column: cross-section morphology.

Table 1
Analysis of relative surface area and porosity of the three types of samples

Sample	BET relative surface area ($m^2\ g^{-1}$)	Pore volume ($cm^3\ g^{-1}$)	Average pore diameter (nm)
SE	2.3047	0.000578	12.5
SEG1	0.0122	0.000016	32.34
SEG2	1.1529	0.001069	312.9

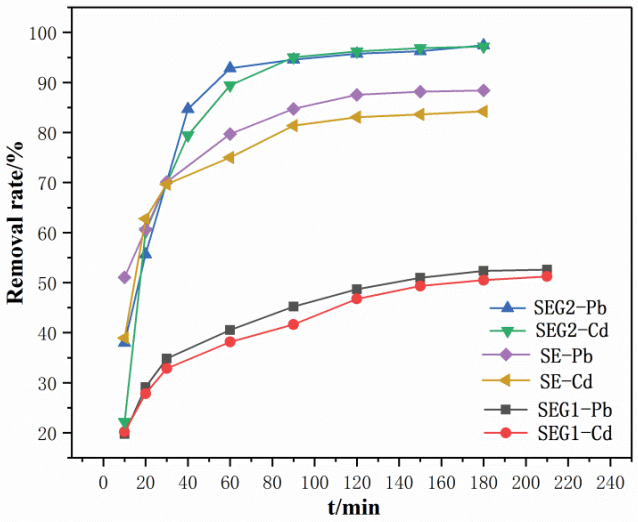

Fig. 2. Removal rates of SE, SEG1, SEG2 toward Pb^{2+} and Cd^{2+} ions at the different adsorption time.

3.2.2. SEG3

SEG3 is a kind of membrane-like material. It is used as filter in a vacuum filter equipped. A volume of 160 mL aqueous solutions containing 10 mg L^{-1} Pb^{2+} and Cd^{2+} ions are filtered through the membrane. Afterwards the concentrations of the Pb^{2+} and Cd^{2+} ions in the liquid phase of the solution are analyzed using inductively coupled plasma atomic emission spectroscopy. Due to the nanometer-sized pores, the filtration through SEG3 membrane is very difficult. According to the experiments and calculation, the amount of water flux through the membrane is only 10.6 L m^{-2} h^{-1} bar^{-1}. At the end, the removal rate toward Pb^{2+} ions is 99.06%; whilst for Cd^{2+} 86.37% can be achieved.

3.2.3. Effect of different ratios of GO, sodium alginate, and EDTA in SEG2 foam

The effect of different ratios of GO, sodium alginate, and EDTA is optimized by changing their contents, respectively. S1, S2, S3, S4, and S5 are prepared by varying the quality of sodium alginate (0.05, 0.1, 0.25, 0.4, and 0.55 g) while keeping the GO (6 g L^{-1}, and 1 mL), twice-distilled water (9 mL) and EDTA (0.2 g) constant. As seen in Fig. 3, the removal rates of Pb^{2+} and Cd^{2+} by GO increases gradually, reach the maximum value at 0.4 g and then decrease. Then, varying the quality of EDTA (0.05, 0.1, 0.2, 0.3, and 0.4 g) while

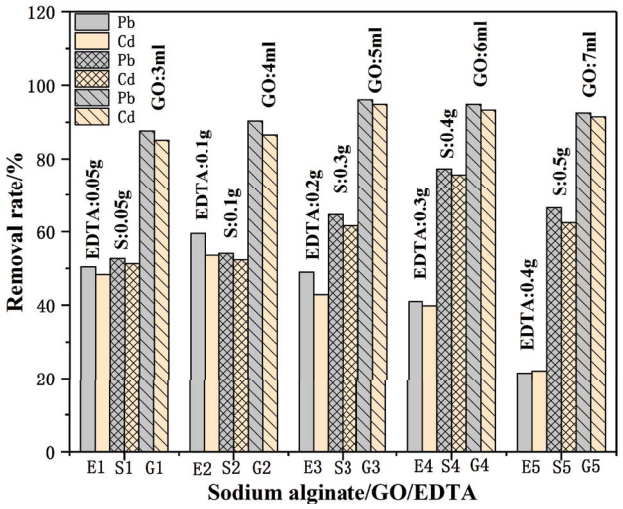

Fig. 3. Removal rates of SEG2 toward Pb^{2+} and Cd^{2+} ions with respect to different mixture ratios. The gray bars indicate the removal rate toward Pb^{2+} ions; whilst the light yellow bars are the ones toward Cd^{2+} ions. For synthesis composites named with the initial letter 'E', the quantities of EDTA are varied from 0.05 (E1), 0.1 (E2), 0.2 (E3), 0.3 (E4), to 0.4 g (E5); while keeping other components constant amount. Similarly, for synthesis composites named with the initial letters 'S' and 'G', the quantities of sodium alginate and GO are, respectively, varied.

keeping the sodium alginate (0.4 g), GO (6 g L^{-1}, and 1 mL) and twice-distilled water (9 mL), the removal rates of Pb^{2+} and Cd^{2+} are similar to change the ratio of sodium alginate. As seen E1, E2, E3, E4, and E5 in Fig. 3, the maximum values are at 0.1 g EDTA (E2). Finally, the influence of different volume GO are studied. 0.4 g sodium alginate and 0.1 g EDTA are added into GO solution (6 g L^{-1}, 3, 4, 5, 6, and 7 mL) and then the solutions are diluted to 10 mL with twice-distilled water. The results are denoted as G1, G2, G3, G4, G5 while the removal rates of Pb^{2+} and Cd^{2+} reach 96.1% and 94.9% at GO 5 mL in Fig. 3. G3.

3.2.4. Effect of pH

The influence of adsorbent dose on the removal of Pb^{2+}, Cd^{2+} ions by SEG2 is investigated in the pH range from 3 to 7. As Fig. 4 shows, the removal rates are low at a lower pH and high at a higher pH. The adsorption capacities of the SEG2 have a significant promoting increase with increasing pH between 3 and 6, whereas the removable rates increase slowly when pH increases from 6 to 7. The lower removal rate under low solution pH can be explained by the competitive adsorption between the Pb^{2+} and Cd^{2+} and hydrogen ions on the limited number of binding sites [15]. Another reason may be attributed to the fact that the carboxyl groups on the SEG2 foam can transform into the carboxylic acid groups at lower pH, which weakens the electrostatic attraction with the cations [16]. Below pH 6, Pb^{2+} is the predominant Pb(II) species. Pb^{2+} and $Pb(OH)^+$ are present in the pH range of 6–7.5. Above pH 7.5, $Pb(OH)^+$ changes to $Pb(OH)_3^-$ and $Pb(OH)_2$ [17]. With further increasing pH from 6 to 7, the hydrogen ions decrease and the SEG2 foam provide more ligands to form complexes with Pb^{2+}, $Pb(OH)^+$

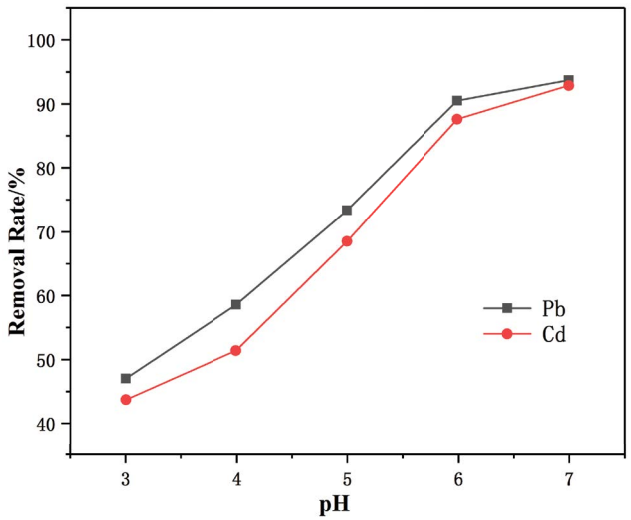

Fig. 4. pH effects on Pb^{2+} and Cd^{2+} adsorbed by SEG2 298 K, contact time 180 min, 10 mL solution with Pb^{2+} and Cd^{2+} initial concentration of 20 mg L^{-1}, respectively.

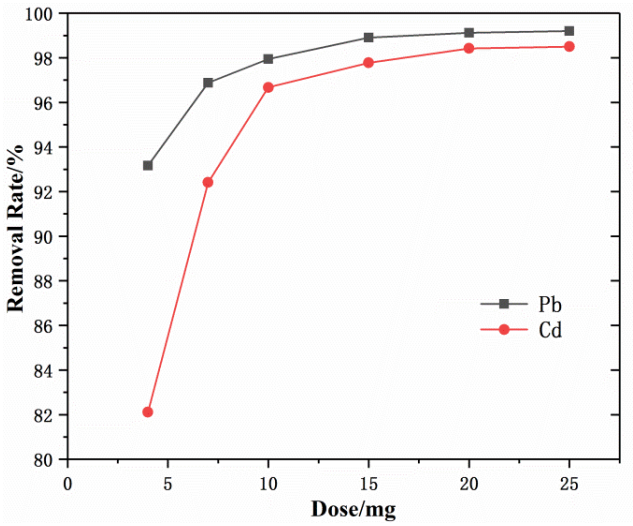

Fig. 5. Effect of different adsorbent doses of SEG2 on the removal rates. The study is performed at 298 K with an interaction time of 180 min. A 20 mL solution (pH 7) containing 20 mg L^{-1} Pb^{2+} and Cd^{2+} ions is used for the investigation.

and Cd^{2+}, which lead to the adsorption capacity of the two metal ions higher. There is a considerable retarding effect on the adsorption with pH from 6 to 7 which may be due to that the surface hydroxyl groups may exchange a proton with positively charged metal species in aqueous solution.

3.2.5. Effect of dose

To optimize the adsorbent dose for the removal of Pb^{2+} and Cd^{2+} from its aqueous solutions, adsorption is carried out with the dose ranging from 4 to 25 mg in 20 mL solution. As Fig. 5 shows, it can be seen that both removal rate of Pb^{2+} and Cd^{2+} rise with increasing the adsorption dose in the initial stage, which may be owing to the existence of a large number of active adsorption sites [18]. Further increase of the adsorbents from 10 to 25 mg has little effect on the removal rate. This may be due to the fact that the SEG2 can provide enough adsorption sites for the complete adsorption of Pb^{2+} and Cd^{2+} ions. Thus, 0.5 g L^{-1} as the ratio of the adsorbent dose and the solution volume is used in the next experiments.

3.2.6. Adsorption kinetics of SEG2

Due to the extraordinary performance of SEG2 in removing Pb^{2+} and Cd^{2+} ions, we further study their adsorption kinetics using pseudo-first-order (Eq. (3)) and pseudo-second-order (Eq. (4)) reaction models shown below [19,20]:

$$\log\left(q_e - q_t\right) = \log q_e - \frac{k_1 t}{2.303} \tag{3}$$

$$\frac{t}{q_e} = \frac{1}{q_e^2 k_2} + \frac{t}{q_e} \tag{4}$$

where q_e (mg g^{-1}) is the amount of adsorption at the equilibrium, q_t (mg g^{-1}) is the adsorbent at time t, k_1 (min^{-1}) is the kinetic rate constant of the pseudo-first-order reaction, and k_2 (g mg^{-1} min^{-1}) is the kinetic rate constant of the pseudo-second-order reaction.

The adsorption rates of Pb^{2+} and Cd^{2+} ions of different initial concentrations onto SEG2 are compared by fitting the adsorption processes with either Eqs. (3) or (4). The fitting parameters are shown in Tables 2 and 3.

As can be seen in Table 2, the adsorption rates of Pb^{2+} ions of different initial concentrations can be fitted using both reaction models. However with the pseudo-second-order reaction model, the fitting is much closer to the experimental results as the R^2 value is nearly 1. This result indicates that the adsorption kinetics of Pb^{2+} ions onto SEG2 has a pseudo-second-order and the chemical adsorption is the rate-control step.

Similar to the Pb^{2+} ions, the adsorption kinetics of Cd^{2+} ions can also be better fitted using the pseudo-second-order reaction model, which indicates that chemical adsorption is the rate-controlling step.

3.3. Comparison and discussion of the adsorbent performance

Comparing the removal rates of the four tested materials toward both Pb^{2+} and Cd^{2+} ions, one can clearly see that the performance of SEG2 is the best. Although SEG3 seem to show the highest removal rate toward Pb^{2+} ions, it is less satisfactory for the case of Cd^{2+} ions. The worst performance is seen when SEG1 is used. Its removal rates toward Pb^{2+} and Cd^{2+} ions are only 54% and 52.7% of the respective performances shown by SEG2. The main cause could be due to the smallest relative surface area of the SEG1 gel spheres, which is 94.5 times less than that of SEG2. Intriguingly SE, the material with the largest relative surface area, does not show prominent adsorption efficiency as well as compared with SEG2. This phenomenon can be understood by considering the different adsorption mechanisms. In SEG2 the graphene oxide can provide large range π-conjugated electrons and

Table 2
Kinetic parameters for the adsorption of Pb^{2+} ions onto SEG2

Initial concentration (mg L^{-1})	Pseudo-first-order kinetics			Pseudo-second-order kinetics		
	k_1 (min^{-1})	q_e (mg g^{-1})	R^2	k_2 (g mg^{-1} min^{-1})	q_e (mg g^{-1})	R^2
10	–0.0278	10.01	0.90982	0.0471	19.16	0.99658
20	–0.0315	34.01	0.97685	0.02227	16.86	0.99584
30	–0.0317	58.343	0.97222	0.0151	13.9	0.99885

Table 3
Kinetic parameters for the adsorption of Cd^{2+} ions onto SEG2

Initial concentration (mg L^{-1})	Pseudo-first-order kinetics			Pseudo-second-order kinetics		
	k_1 (min^{-1})	q_e (mg g^{-1})	R^2	k_2 (g mg^{-1} min^{-1})	q_e (mg g^{-1})	R^2
10	–0.039	19.2	0.98822	0.04817	16.7	0.99874
20	–0.0328	37.98	0.99335	0.02145	18.7	0.99468
30	–0.0221	44.63	0.98859	0.0151	13.9	0.99868

rich amount of oxygen-containing functional groups. These chemical properties enable the adsorption of heavy metal ions onto SEG2 not only through physical process but also via chemical interactions. For example, the delocalized π electron systems of the GO act as the Lewis base while the heavy metal ions can act as the Lewis acid. The delocalized π electron systems can form electron donor–acceptor complexes with heavy metal ions through the Lewis acid–base interaction [21,22]. In addition, the adsorption of heavy metal ions on SEG2 foam has complexation because of the existence of EDTA.

The synthesized composites seem to have higher adsorption performance toward Pb^{2+} than for Cd^{2+} ions, which could be due to their different material property dependent affinities with the adsorbents [23,24]. The radii of the Pb^{2+} and Cd^{2+} ions are 1.19 and 0.95 Å, respectively. The larger the ion radius, the easier they can be blocked by the porous adsorbents. Furthermore, the electric negativities of the Pb^{2+} and Cd^{2+} ions are 2.33 and 1.69, respectively. It has been reported that ions with large electric negativity are easier to form stable complex with the oxygen-containing functional groups via the lone-pair electrons [25,26]. This could be a further reason for understanding the higher removal rate of Pb^{2+} ions than for Cd^{2+} ions.

The adsorption processes of SE, SEG1, SEG2 reach an equilibrium state in different time and the shortest time is SEG2. It could be due to the largest pore diameter of the SEG2 foam except the strong attractive forces between heavy metal ions and the sorbent, which is favorable for facilitating the interstitial diffusion of heavy metal ions to active sites [27–29].

4. Conclusions

Four types adsorbent are synthesized by mixing SA, EDTA, and GO with different methods. The SEM and relative surface area analysis show that the compounds possess three-dimensional network structures. Especially SEG2 has regular porous morphology with high mechanical strength. At room temperature and a pH value of 7, it shows the highest removal efficiency toward Pb^{2+} and Cd^{2+} ions with the removal rates as 97.44% and 97.16%, respectively. This outstanding removal performance of SEG2 is due to the synergy of physical adsorption as well as chemical adsorption processes.

Acknowledgments

The authors gratefully acknowledge the financial support provided by the Key Scientific Research Project Plan of Henan Higher Education Institutions (16A610007), the Scientific and Technological Key Projects in Henan Province (182102310847) and the Scientific Research Capability Upgrading Project in Henan University of Urban Construction (2017YY048).

References

[1] J. Morton, N. Havens, A. Mugweru, A.K. Wanekaya, Detection of trace heavy metal ions using carbon nanotube- modified electrodes, Electroanalysis, 21 (2010) 1597–1603.
[2] C.K. Jain, D.C. Singhal, M.K. Sharma, Adsorption of zinc on bed sediment of River Hindon: adsorption models and kinetics, J. Hazard. Mater., 114 (2004) 231–239.
[3] M. Sekar, V. Sakthi, S. Rengaraj, Kinetics and equilibrium adsorption study of lead(II) onto activated carbon prepared from coconut shell, J. Colloid Interface Sci., 279 (2004) 307–313.
[4] N. Kongsricharoern, C. Polprasert, Chromium removal by a bipolar electro-chemical precipitation process, Water Sci. Technol., 34 (1996) 109–116.
[5] S. Rengaraj, K.-H. Yeon, S.-H. Moon, Removal of chromium from water and wastewater by ion exchange resins, J. Hazard. Mater., 87 (2001) 273–287.
[6] J. Zhao, W. Ren, H.-M. Cheng, Graphene sponge for efficient and repeatable adsorption and desorption of water contaminations, J. Mater. Chem., 22 (2012) 20197–20202.
[7] Z. Reddad, C. Gerente, Y. Andres, P. Le Cloirec, Adsorption of several metal ions onto a low-cost biosorbent: kinetic and equilibrium studies, Environ. Sci. Technol., 36 (2002) 2067–2073.
[8] S.E. Bailey, T.J. Olin, R.M. Brick, D.D. Adrian, A review of potentially low-cost sorbents for heavy metals, Water Res., 33 (1999) 2469–2479.

[9] W.C. Wan, R.Y. Zhang, W. Li, H. Liu, Y.H. Lin, L.N. Li, Y. Zhou, Graphene–carbon nanotube aerogel as an ultra-light, compressible and recyclable highly efficient absorbent for oil and dyes, Environ. Sci.: Nano, 3 (2016) 107–113.
[10] H. Wang, Y.G. Liu, G.M. Zeng, X.J. Hu, X. Hu, T.T. Li, H.Y. Li, Y.Q. Wang, L.H. Jiang, Grafting of β-cyclodextrin to magnetic graphene oxide via ethylenediamine and application for Cr(VI) removal, Carbohydr. Polym., 113 (2014) 166–173.
[11] W. Gao, L.B. Alemany, L.J. Ci, P.M. Ajayan, New insights into the structure and reduction of graphite oxide, Nat. Chem., 1 (2009) 403–408.
[12] W.W. Cai, R.D. Piner, F.J. Stadermann, S.J. Park, M.A. Shaibat, Y. Ishii, D.X. Yang, A. Velamakanni, S.J. An, M. Stoller, J. An, D.M. Chen, R.S. Ruoff, Synthesis and solid-state NMR structural characterization of ^{13}C-labeled graphite oxide, Science, 321 (2008) 1815–1817.
[13] T.F. Huang, L. Zhang, H.L. Chen, C.J. Gao, Sol–gel fabrication of a non-laminated graphene oxide membrane for oil/water separation, J. Mater. Chem. A, 3 (2015) 19517–19524.
[14] R.L.D. Whitby, A. Korobeinyk, S.V. Mikhalovsky, T. Fukuda, T. Maekawa, Morphological effects of single-layer graphene oxide in the formation of covalently bonded polypyrrole composites using intermediate diisocyanate chemistry, J. Nanopart. Res., 13 (2011) 4829–4837.
[15] L. Liu, Y. Wan, Y. Xie, R. Zhai, B. Zhang, J. Liu, The removal of dye from aqueous solution using alginate-halloysite nanotube beads, Chem. Eng. J., 187 (2012) 210–216.
[16] Q. Li, Y.H. Li, X.M. Ma, Q.J. Du, K.Y. Sui, D.C. Wang, C.P. Wang, H.L. Li, Y.Z. Xia, Filtration and adsorption properties of porous calcium alginate membrane for methylene blue removal from water, Chem. Eng. J., 316 (2017) 623–630.
[17] K.G. Sreejalekshmi, K.A. Krishnan, T.S. Anirudhan, Adsorption of Pb(II)and Pb(II)-citric acid on sawdust activated carbon: kinetic and equilibrium isotherm studies, J. Hazard. Mater., 161 (2009) 1506–1513.
[18] N. Song, X.-L. Wu, S.X. Zhong, H.J. Lin, J.-R. Chen, Biocompatible G-Fe_3O_4/CA nanocomposites for the removal of Methylene Blue, J. Mol. Liq., 212 (2015) 63–69.
[19] A.R. Cestari, E.F.S. Vieira, J.D.S. Matos, D.S.C. dos Anjos, Determination of kinetic parameters of Cu(II) interaction with chemically modified thin chitosan membranes, J. Colloid Interface Sci., 285 (2005) 288–295.
[20] L.L. Li, L.L. Fan, M. Sun, H.M. Qiu, X.J. Li, H.M. Duan, C.N. Luo, Adsorbent for chromium removal based on graphene oxide functionalized with magnetic cyclodextrin–chitosan, Colloids Surf., B, 107 (2013) 76–83.
[21] V. Georgakilas, M. Otyepka, A.B. Bourlinos, V. Chandra, N. Kim, K.C. Kemp, P. Hobza, R. Zboril, K.S. Kim, Functionalization of graphene: covalent and non-covalent approaches, derivatives and applications, Chem. Rev., 112 (2012) 6156–6214.
[22] P. Tan, J. Sun, Y.Y. Hu, Z. Fang, Q. Bi, Y.C. Chen, J.H. Cheng, Adsorption of Cu^{2+}, Cd^{2+} and Ni^{2+} from aqueous single metal solutions on graphene oxide membranes, J. Hazard. Mater., 297 (2015) 251–260.
[23] Z.M. Gao, T.J. Bandosz, Z.B. Zhao, M. Han, J.S. Qiu, Investigation of factors affecting adsorption of transition metals on oxidized carbon nanotubes, J. Hazard. Mater., 167 (2009) 357–365.
[24] C. Liu, R. Bai, Q. San Ly, Selective removal of copper and lead ions by electronegativity, J. Am. Chem. Soc., 105 (1983) 7512–7516.
[25] C. Liu, R. Bai, Q. San Ly, Selective removal of copper and lead ions by diethylenetriamine-functionalized adsorbent: behaviors and mechanisms, Water Res., 42 (2008) 1511–1522.
[26] P. Tan, Y. Hu, Q. Bi, Competitive adsorption of Cu^{2+}, Cd^{2+} and Ni^{2+} from an aqueous solution on graphene oxide membranes. Colloids Surf., A, 509 (2016) 56–64.
[27] Y. Yang, Y. Xie, L. Pang, M. Li, X. Song, J. Wen, H. Zhao, Preparation of reduced graphene oxide/poly(acrylamide) nanocomposite and its adsorption of Pb(II) and methylene blue, Langmuir, 29 (2013) 10727–10736.
[28] G. Zhao, J. Li, X. Ren, C. Chen, X. Wang, Few-layered graphene oxide nanosheets as superior sorbents for heavy metal ion pollution management, Environ. Sci. Technol., 45 (2011) 10454–10462.
[29] V. Antochshuk, M. Jaroniec, 1-Allyl-3-propylthiourea modified mesoporous silica for mercury removal, Chem. Commun., 7 (2002) 258–259.